The Astrophysical Journal, 834:83 (13pp), 2017 January 1 doi:10.3847/1538-4357/834/1/83

NO OVERDENSITY OF LYMAN-ALPHA EMITTING GALAXIES AROUND A QUASAR AT $z \sim 5.7$

C. Mazzucchelli[1], E. Bañados[1,2,4], R. Decarli[1], E. P. Farina[1], B. P. Venemans[1], F. Walter[1], and R. Overzier[3]
[1] Max Planck Institute für Astronomy, Königstuhl 17, D-69117 Heidelberg, Germany
[2] The Observatories of the Carnegie Institute of Washington, 813 Santa Barbara Street, Pasadena, CA 91101, USA
[3] Observatório Nacional, Rua José Cristino, 77. CEP 20921-400, São Cristóvão, Rio de Janeiro-RJ, Brazil
Received 2015 December 4; revised 2016 October 12; accepted 2016 November 7; published 2017 January 4

ABSTRACT

Bright quasars, observed when the universe was less than one billion years old ($z > 5.5$), are known to host massive black holes ($\sim 10^9\,M_\odot$) and are thought to reside in the center of massive dark matter overdensities. In this picture, overdensities of galaxies are expected around high-redshift quasars. However, observations based on the detection of Lyman-break galaxies (LBGs) around these quasars do not offer a clear picture: this may be due to the uncertain redshift constraints of LBGs, which are solely selected through broadband filters. To circumvent such uncertainties, we here perform a search for Lyman-alpha emitting galaxies (LAEs) in the field of the quasar PSO J215.1512–16.0417 at $z \sim 5.73$, through narrowband deep imaging with FORS2 at the Very Large Telescope. We study an area of 37 arcmin^2, i.e., $\sim$206 comoving Mpc^2 at the redshift of the quasar. We find no evidence of an overdensity of LAEs in the quasar field with respect to blank-field studies. Possible explanations for these findings may be that our survey volume is too small, or that the strong ionizing radiation from the quasar hinders galaxy formation in its immediate proximity. Another possibility is that these quasars are not situated in the dense environments predicted by some simulations.

Key words: cosmology: observations – galaxies: high-redshift – quasars: individual (PSO J215.1512–16.0417)

1. INTRODUCTION

Quasars are among the most luminous sources in the universe, hosting supermassive black holes (as massive as $M_{\rm BH} \gtrsim$ few $\times\ 10^8\,M_\odot$) that reside in the center of massive galaxies. Quasars have been observed at high redshift ($z \gtrsim 5.5$, e.g., Fan et al. 2006; Willott et al. 2010; Morganson et al. 2012; Bañados et al. 2014, 2016; Carnall et al. 2015) up to $z \sim 7$ (e.g., Mortlock et al. 2011; Venemans et al. 2013, 2015). Metallicity estimates based on the intensity of broad emission lines (e.g., Barth et al. 2003; De Rosa et al. 2011) and observations of dust and molecular gas reservoirs (e.g., Walter et al. 2003; Maiolino et al. 2005; Riechers et al. 2009; see for a review Carilli & Walter 2013) suggest that the host galaxies of these quasars have experienced sufficient star formation to pollute the interstellar medium with metals, up to close-to-solar abundances. The presence of apparently evolved systems so early in the history of the universe (i.e., $\sim$1 Gyr from the Big Bang) sets constraints on the current scenario of structure formation and galaxy evolution. Models of massive black hole formation in the early universe invoke the direct collapse of a massive gaseous reservoir (e.g., Heahnelt & Rees 1993; Begelman et al. 2006; Latif & Schleicher 2015), the creation of black hole seeds from the collapse of Population III stars (e.g., Bond et al. 1984), or the interplay between gas collapse, star formation, and dynamical processes (e.g., Devecchi & Volonteri 2009; see for a review Volonteri 2010). In all these cases, the process of gas cooling and fragmentation drives the formation of both massive black holes and stars. A coexistence of fast-accreting black holes and star-forming galaxies is thus expected at these very early cosmic epochs. In addition, mergers among these galaxies may funnel black hole growth and could explain the onset of the black hole—host galaxy scaling relations (see, e.g., Jahnke & Macció 2011). The subsequent relation observed between the latter and the hosting dark matter halo suggests that these high-z quasars, harboring black holes of $\sim 10^9\,M_\odot$, are expected to reside in massive dark matter halos of $\sim 10^{13}\,M_\odot$ (e.g., Ferrarese 2002; Wyithe & Loeb 2003), where a large number of galaxies are also expected to form (Overzier et al. 2009). These structures can eventually evolve into large gravitationally bound systems in the present universe (with a large scatter in mass, from groups to clusters, e.g., Springel et al. 2005; Overzier et al. 2009; Angulo et al. 2012). Observational attempts to detect these high-redshift galaxies in the vicinities of high-redshift quasars complement the aforementioned theoretical predictions. One of the most efficient and successful methods to identify high-redshift galaxies is through the Lyman-break technique (drop-outs or Lyman-break galaxies, LBGs): absorption by neutral hydrogen causes a break in the observed galactic spectrum; this is apparent by an abrupt change in colors (e.g., Steidel et al. 1996).

A number of studies investigated the presence of the theoretically expected galaxies around $z \sim 6$ quasars, using the Lyman-break technique. However, the picture sketched out by observations is far from clear. For instance, Stiavelli et al. (2005) found an overdensity of LBGs in the field of the bright $z \sim 6.28$ quasar SDSS J1030+0524, based on i_{775} and z_{850} images taken with the Advanced Camera for Surveys (ACS) at the *Hubble Space Telescope* (*HST*, with a field of view of $\sim$11 arcmin^2, corresponding to an area of $\sim$65 comoving Mpc^2 [cMpc^2] at $z \sim 6$). On the other hand, Kim et al. (2009) studied the environment of five $z \sim 5$ quasars, again searching for LBGs through *HST* ACS imaging: they estimated that the fields around two quasars are overdense, two are underdense, and one is consistent with a blank field. Simpson et al. (2014) investigated the environment of the most distant quasar to date, ULAS J1120+0641 ($z \sim 7$), but recovered no evidence of an overdensity of galaxies (using data from *HST* ACS). Studies on scales larger than ACS *HST* do not provide an unambiguous scenario either. Utsumi

[4] Carnegie-Princeton Fellow.

et al. (2010) found an enhancement in the number of LBGs in the field of the quasar CFHQS J2329–0301 ($z \sim 6.4$), which was observed with the Suprime Camera at the Subaru Telescope, whose field of view covers an area of ∼900 arcmin^2 (∼4600 cMpc^2). Recently, Morselli et al. (2014) showed that four $z \sim 6$ quasars were situated in overdense environments, based on a search for LBGs with deep multiwavelength photometry from the Large Binocular Camera (LBC) at the Large Binocular Telescope (whose field of view covers a wide area of ∼575 arcmin^2 ∼3100 cMpc^2). Conversely, Willott et al. (2005) imaged three SDSS quasars at $z > 6$ with GMS-North on the Gemini-North Telescope (whose field of view is ∼30 arcmin^2, amounting to ∼170 cMpc^2 at $z \sim 6$), but recovered no clear signs of an overdensity of LBGs.

The different findings may be ascribed to different reasons, e.g., the depths reached in the observations, diverse considered techniques/selection criteria, different probed survey areas (and therefore scales), and the diverse inspected fields, which may be intrinsically different. More importantly, the Lyman-break technique, using broadband filters whose passbands normally span $\Delta\lambda \sim 1000$ Å, does not provide an accurate redshift determination ($\Delta z \sim 1$, equals to line-of-sight distances $\Delta d \sim 850$ cMpc or 120 physical Mpc [pMpc] at $z \sim 6$). Any possible overdensity may be diluted over this large cosmological volume (Chiang et al. 2013), taking into account that the universe is homogeneous at scales $\gtrsim$70–100 h^{-1} Mpc (Wu et al. 1999; Sarkar et al. 2009). Samples of photometric LBGs, selected without a large number of broadband filters, are likely to be contaminated by foreground sources (e.g., lower-z, red/dusty galaxies).

A more secure approach to identify high-redshift galaxies is to search for sources with a bright Lyα emission (Lyman-alpha emitters, LAEs). Such narrow line emission can be recovered by specific narrowband filters ($\Delta\lambda \sim 100$ Å). An immediate advantage, with respect to the LBG selection, is that the covered redshift range is much narrower ($\Delta z \sim 0.1$, corresponding to $\Delta d \sim 44$ cMpc ∼ 7 pMpc at $z \sim 6$), i.e., an overdensity membership can be clearly established. LAEs are believed to be mostly low-mass galaxies, spanning a range of stellar masses of $\sim 10^6$–$10^8\,M_\odot$ and ages of ∼1–3 Myr (e.g., Pirzkal et al. 2007; Ono et al. 2010). However, a non-negligible fraction of massive galaxies (with masses of up to $\sim 10^{11}\,M_\odot$) and galaxies hosting older stellar population (∼1 Gyr) has also been found among LAEs (e.g., Finkelstein et al. 2009, 2015; Pentericci et al. 2009). Bañados et al. (2013, hereafter B13) carried out the first and, until the present work, only search for LAEs at scales $\gtrsim$1 pMpc around a $z > 5.5$ quasar.[5] They used a collection of broadband and narrowband filters at the Very Large Telescope (VLT). No strong evidence was found of an enhancement in the number of LAEs with respect to the blank field.

Here we present a search for LAEs in the field around the broad absorption line quasar PSO J215.1512–16.0417 (hereafter PSO J215–16). It has a bolometric luminosity of 3.8×10^{47} erg s^{-1}, with 0.2 dex of uncertainty, and a black hole mass of $6.7 \times 10^9\,M_\odot$, with an uncertainty of 0.3 dex. The redshift is $z = 5.732 \pm 0.007$, measured from the OI emission line ($\lambda_{\rm rest} = 1307$ Å). This line is the brightest and clearest of the emission lines observed in the spectrum of the quasar. As a further check, other emission lines were fitted (N V, S II, and C II). The obtained redshift estimates are consistent (with a scatter of ∼0.02) within the astrophysical systematic uncertainties (Morganson et al. 2012). The structure of this paper is as follows: we describe the observations and data reduction in Section 2. In Section 3 we present our LAE selection criteria. In Section 4 we study the environment of the quasar on the base of the candidates found in the previous section. In Section 5 we simulate a population of $z \sim 5.7$ LAEs to which we compare our results. In Section 6 we place our work in the context of the current clustering studies. In Section 7 we discuss our results. Finally, in Section 8 we present our conclusions and outline possible future steps. All magnitudes reported here are in the AB system and corrected for the galactic dust extinction following Schlafly & Finkbeiner (2011). We use a ΛCDM cosmology, with $H_0 = 70$ km s^{-1} Mpc^{-1}, $\Omega_{\rm M} = 0.3$, and $\Omega_\Lambda = 0.7$: this implies that 1 arcmin ∼2.36 cMpc ∼0.35 pMpc at $z = 5.73$ (the redshift of the quasar studied here).

2. OBSERVATIONS AND DATA REDUCTION

We obtained multiwavelength photometry of the field around the quasar PSO J215–16 with the FOcal Reducer/low dispersion Spectrograph 2 (FORS2, Appenzeller & Rupprecht 1992) at the VLT. The observations were obtained over nine nights in 2013, June, July, and August. We used the red sensitive detector consisting of two 2k × 4k MIT CCDs. In order to decrease the readout time and noise, we adopted a 2 × 2 binning. The resulting pixel size is 0.25 arcsec/pixel, and the total field of view is equal to 6.8 × 6.8 arcmin^2, i.e., 2.38 × 2.38 pMpc^2.

We collected images in two broadband filters R_SPECIAL (R, with a central wavelength $\lambda_c = 6550$ Å, and a width $\Delta\lambda = 1650$ Å) and z_GUNN (z, $\lambda_c = 9100$ Å, $\Delta\lambda = 1305$ Å), and in the narrowband filter FILT815_13+70 (NB, $\lambda_c = 8150$ Å, $\Delta\lambda = 130$ Å). The filters allow us to select LAEs at redshifts between $5.66 \lesssim z \lesssim 5.75$ ($\Delta z \sim 0.1$), i.e., at the precise redshift of the quasar studied here. With the broadband filters, LBGs can be selected in a redshift range of $5.2 \lesssim z \lesssim 6.5$ ($\Delta z \sim 1.3$). The filter throughputs, together with a synthetic LAE spectrum at the redshift of the quasar, are shown in Figure 1.

The individual exposure times in each frame are 240 s in R, 115 s in z, and 770 s in NB. Each exposure was acquired with a dithering of ∼10″ in order to account for bad pixels and remove cosmic rays. The total exposure times are ∼1.13, 2.11, and 8.56 hr in the R, z, and NB filter, respectively.

We perform a standard data reduction: we subtract from each exposure the bias, we apply the flat field, and we subtract the background, then the images are aligned and finally combined; the astrometric solution was derived with `astrometry.net` (Lang et al. 2010). A composite RGB image of the quasar field is shown in Figure 2.

The seeing values of the stacked images are equal to 0.″78 in R, 0.″81 in z, and 0.″79 in NB. In order to circumvent uncertainties due to different apertures or to the angular resolution of the images, we match the point-spread function (PSF) of the R and NB images to the one of the z filter frame (the one with the worst seeing) using the IRAF task Gauss. We calculate the photometry using as reference sources field stars retrieved from the Pan-STARRS1 catalog (Magnier et al. 2013). We calculate the conversion between the two different filter sets by interpolating spectra of standard stars. The

[5] Previously, Decarli et al. (2012) also searched for Lyα emission around two $z > 6$ quasars through narrowband imaging with *HST*, but their study was limited to far smaller scales (∼1 arcmin ∼0.35 pMpc).

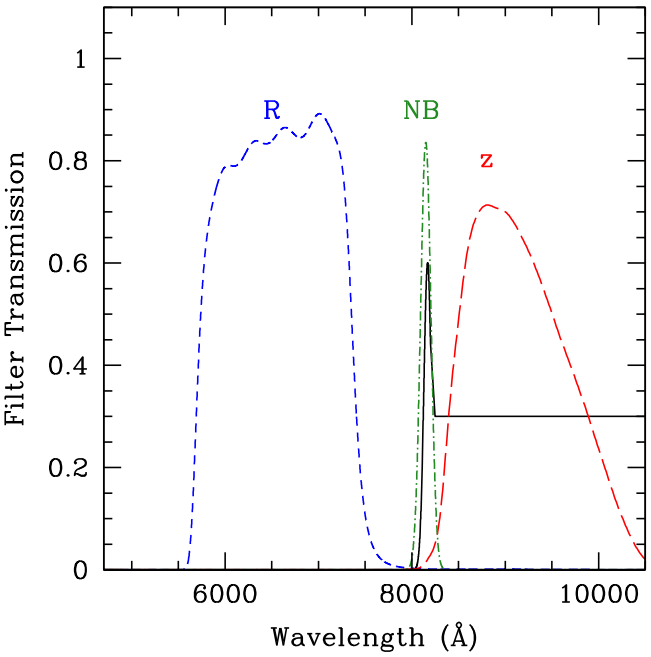

Figure 1. Set of filters used in the present study, R_SPECIAL (*R*, short dashed blue line), z_GUNN (*z*, long dashed red line) and the Narrowband filter FILT815_13+70 (NB, dot–dashed green line). We show as a solid black line a synthetic spectrum of a Lyman-alpha emitter (LAE) at the redshift of the quasar studied in this work ($z \sim 5.7$).

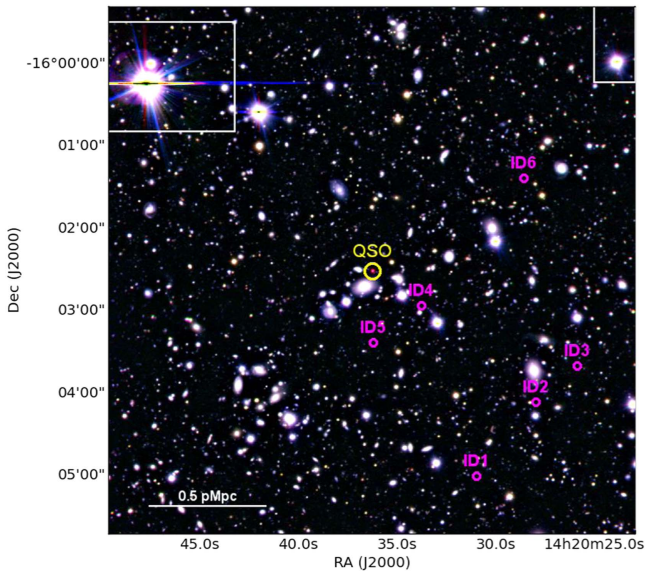

Figure 2. RGB composite image of the field around the quasar PSO J215–16. In magenta we show the position of the sources that were only observed in the narrow band, but not detected (at 2σ confidence level) in the *R* and *z* filters (see Section 3, Figure 3, and Table 1.). The position of the quasar and masked regions around bright stars are also shown. The total analyzed area is 37 arcmin^2.

relations are

$$R = r_{\rm P1} - 0.277 \times (r_{\rm P1} - i_{\rm P1}) - 0.005, \quad (1)$$

$$z = z_{\rm P1} - 0.263 \times (z_{\rm P1} - y_{\rm P1}) - 0.001, \quad (2)$$

$$\mathrm{NB} = i_{\rm P1} - 0.626 \times (i_{\rm P1} - z_{\rm P1}) + 0.014, \quad (3)$$

where $r_{\rm P1}$, $i_{\rm P1}$, $z_{\rm P1}$, and $y_{\rm P1}$ are the magnitudes in the Pan-STARRS1 filters.

The obtained zero-point values are 27.77 ± 0.04 in *R*, 27.12 ± 0.02 in *z*, and 24.85 ± 0.04 in the NB filter. We calculate the noise in our images by computing the standard deviation of flux measurements in circular apertures with a radius of 3 pixels that were placed randomly in empty regions in the images. This is the radius of the aperture over which we perform our photometry, as discussed below. We achieve limit magnitudes at 5σ level of 26.47, 25.96, and 26.38 mag in the *R*, *z,* and NB frames.

In order to identify sources from the images, we use the software `SExtractor` (Bertin & Arnouts 1996) in the double-image mode, requiring a minimum detection threshold of 1.8σ. Since we expect LAEs to be strongly detected in the NB filter, we take this frame as the base of our selection. We cut the outskirts of the frames and mask saturated stars, where both the astrometry and the photometry were less reliable. The final effective area is equal to 37 arcmin^2 (i.e., $\sim$206 cMpc^2 at the redshift of the quasar).

We perform the photometry of the sources over an aperture with a radius of 3 pixels (0.″75). For our frames this is equal to $1.8\times$ seeing: i.e., we encompass more than $\sim$90% of the flux, and at the same time maximize the signal-to-noise ratio.

We consider only sources with a signal-to-noise ratio S/N > 4 in the NB filter and adopt a 2σ upper limit in *R* and *z* for non-detections in the broadband images (27.46 in *R* and 26.95 in *z*). Sources that are non-detected in the broad bands are allowed in the catalog, and we substitute the *R* and *z* values with the respective 2σ limit magnitudes. Finally, we use the "flags" parameter given by `SExtractor` in order to discard unreliable detections, rejecting sources with flags $\geqslant$4 (i.e., saturated or truncated objects, or those whose aperture data are incomplete or corrupted); the final catalog encompasses 3250 sources.

We extrapolate the cumulative count for the sources detected in our NB frame to estimate the completeness function of our study at the faint end (see Figure 3). We compute the logarithmic cumulative number counts of sources detected in NB as a function of NB magnitude. We fit it with a linear relation (in log-mag space) for $21 <$ NB < 25, and extrapolate it toward the faint end. The completeness is computed as the ratio between the expected number counts from the logN-logS extrapolation and the actual number of detected sources. Our catalog reaches a completeness of 80% and 50% at NB magnitudes of 26.3 and 27.1, respectively.

3. SELECTION OF HIGH-REDSHIFT GALAXY CANDIDATES

In this work we follow the color selection defined in B13, which we briefly describe below.

LAEs are expected to be well detected in the narrow band and to show a break in the continuum emission. More precisely, we required our LAE candidates to satisfy the following criteria:

1. (*z*–NB) > 0.75. We request the flux density in the NB to be at least twice the one observed in the *z* filter. This cut implies that we are selecting objects with an equivalent width (EW) of the Lyα line in the restframe greater than 25. Å (see Section 5).
2. (*R*–*z*) > 1.0. We expect lower flux at wavelengths shorter than the Lyα emission line, i.e., a break in the spectrum, which can be identified by requiring a very red *R*–*z* color.

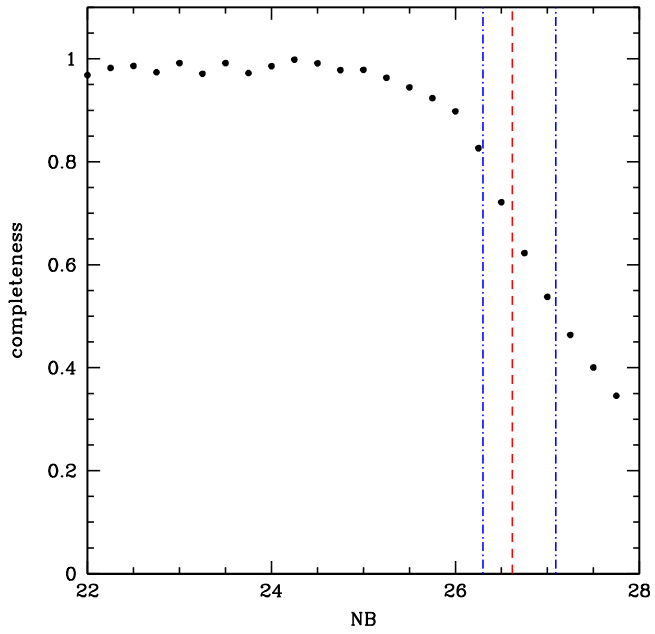

Figure 3. Detection completeness function for the sources in our catalog as a function of NB magnitude (see text for details). With a red long dashed line we show the 4σ limit magnitude estimated from the image noise, which corresponds to a level of completeness of 67%. We show the 80% and 50% completeness levels (at magnitudes of 26.3 and 27.1, respectively), with blue dot–dashed lines.

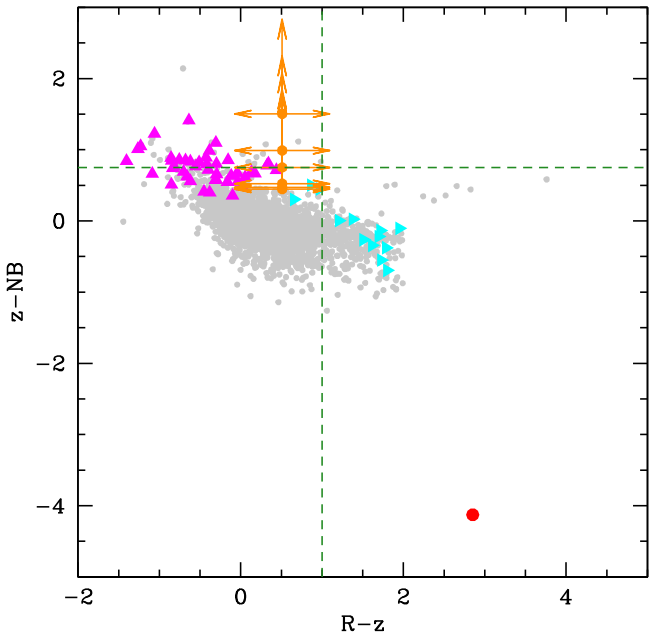

Figure 4. Color–color diagram of the sources in our field detected in the NB filter with S/N > 4. The sources detected with a significance lower than 2σ, only in the z or in the R filter, are shown as magenta and cyan triangles, respectively. Orange arrows indicate objects undetected in either R and z (six sources). Our selection cuts for LAEs are displayed with green dashed lines; LAEs should fall in the upper right panel (see Section 3 for the complete set of our criteria). No LAE candidates are securely found in our field. The red point in the lower right corner corresponds to the quasar.

In case a source is not detected in R or z, we adopt the 2σ limit magnitudes.

3. $|(z - \mathrm{NB})| > 2.5 \times \sqrt{\sigma_z^2 + \sigma_{\mathrm{NB}}^2}$. We wish to select only objects with a significant flux excess in the NB. Therefore, we adopt a constraint in order to discard all the objects that only satisfy our selection criteria through their photometric errors.
4. NB > 18. Since LAEs are expected to be faint sources at these redshifts, we impose a lower limit to the observed NB magnitude. However, we note that there are no objects with NB < 18 that satisfy all the previous criteria.

In Figure 4 we show the (z–NB) versus (R–z) color–color diagram together with our high-redshift galaxy selection. LAEs are expected to fall in the upper right part. In summary, we find no secure detections of LAEs in our field, i.e., no sources fully satisfy all the selection criteria described above. We observe six sources with a detection in the NB that are not detected in the R and z frames. The ($z_{2\sigma,\mathrm{lim}}$-NB) color ranges from a value of 0.45 to 1.5. In the following analysis, we conservatively consider all these six sources as LAE candidates; however, we stress that to determine whether these objects fully satisfy our criteria, deeper R-band and z-band observations are needed.

In Table 1 we report their coordinates, the NB magnitudes, the projected distances from the quasar, the estimated Lyα luminosities, and the star formation rates (SFR; which are within the expectations for typical $z \sim 6$ LAEs, SFR $\sim 6^{+3}_{-2}$ $M_{\odot}\,\mathrm{yr}^{-1}$, Ouchi et al. 2008; see Appendix A). Their postage stamps in the three filters are shown in Figure 5.

4. STUDY OF THE ENVIRONMENT

In order to study the environment of the quasar PSO J215–16, we compare our findings to earlier quasar environment studies and to blank fields (i.e., fields where no quasars are present). In Figure 6 we show the cumulative number counts, rescaled to our effective area (37 arcmin^2), of LAEs found in two blank fields, Ouchi et al. (2008) and Hu et al. (2010), and in the field of another $z \sim 5.7$ quasar, B13. The number counts of the objects found in this work are corrected taking into account the completeness of our catalog at the respective NB magnitude.

Ouchi et al. (2008) and Hu et al. (2010) searched for LAEs at redshift $z = 5.7$ in seven SuprimeCam fields and in the Subaru/*XMM-Newton* Deep Survey, respectively. The total areas covered in the two studies are $\sim$1.16 and $\sim$1 deg^2. The difference between the number counts of these two measurements may be ascribed to the fact that Hu et al. (2010) only considered the spectroscopically confirmed sources in their sample, while the sample of Ouchi et al. (2008) was based on the photometric selection, possibly affected by contaminants, but also characterized by a higher completeness level. The present work and B13 are carried out with the same filter set and instrument, and assuming consistent selection criteria. Even when we were to consider all the sources detected solely in the NB filter in our work as LAE candidates (see Section 3), the number counts would be consistent with the blank-field measurements and with B13.

Therefore, there is no evidence of an overdensity of LAEs at the redshift of the quasar.

5. SIMULATION OF LAE

We estimate the fraction of LAEs that we expect to detect based on observations of blank fields, our filter sets, and our image depths. Given the setup of our observations, we aim to

Table 1
Source Names, Sky Coordinates, NB Magnitudes (AB System), and Projected Distances to the Quasar of the Objects Retrieved in our Field with a Detection in NB (at S/N > 4) and a Non–detection in the Broad Bands

ID	R.A. (J2000.00)	Decl. (J2000.00)	mag_{NB} (AB)	Angular Distance (arcmin)	Comoving Distance (cMpc)	Physical Distance (pMpc)	$L_{Ly\alpha}$ $\times 10^{42}$ (erg s^{-1})	SFR ($M_\odot$ yr^{-1})
ID1	14:20:31.1	−16:04:59.2	26.50 ± 0.22	2.79	6.58	0.98	>1.9 ± 0.4	1.2 ± 0.2
ID2	14:20:28.1	−16:04:05.9	25.45 ± 0.09	2.55	6.00	0.89	>5.1 ± 0.4	3.2 ± 0.3
ID3	14:20:26.0	−16:03:39.7	26.43 ± 0.21	2.74	6.46	0.96	>2.1 ± 0.4	1.3 ± 0.2
ID4	14:20:33.9	−16:02:55.9	25.96 ± 0.14	0.74	1.75	0.26	>3.2 ± 0.4	2.0 ± 0.2
ID5	14:20:36.3	−16;03:23.0	26.20 ± 0.17	0.88	2.08	0.31	>2.5 ± 0.4	1.6 ± 0.2
ID6	14:20:28.7	−16.01:23.8	26.48 ± 0.22	2.14	5.05	0.75	>2.0 ± 0.4	1.2 ± 0.2

Note. We also show the luminosities of the Lyα emission line and the SFRs as estimated in Appendix A. The errors on the SFRs are derived from the photometric uncertainties on the narrowband magnitudes and do not account for systematics in the underlying assumptions.

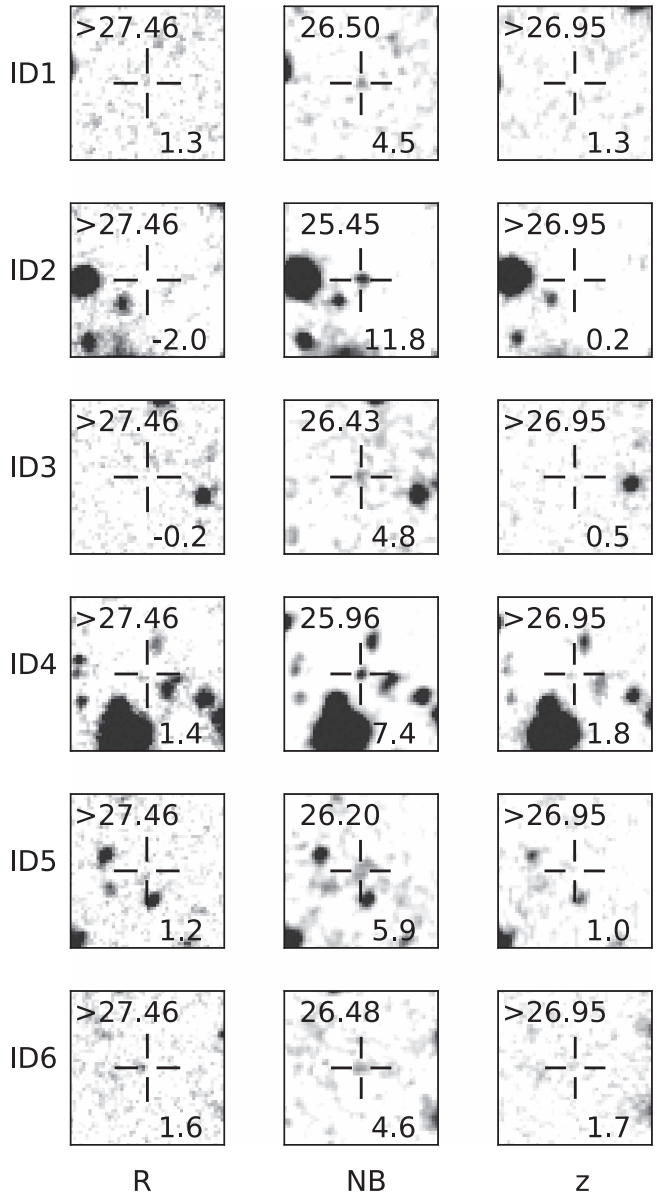

Figure 5. Postage stamps centered on the sources detected only in the NB, in a region of 12″ × 12″. The magnitudes and S/N in the three bands are also reported in top left and bottom right corner, respectively.

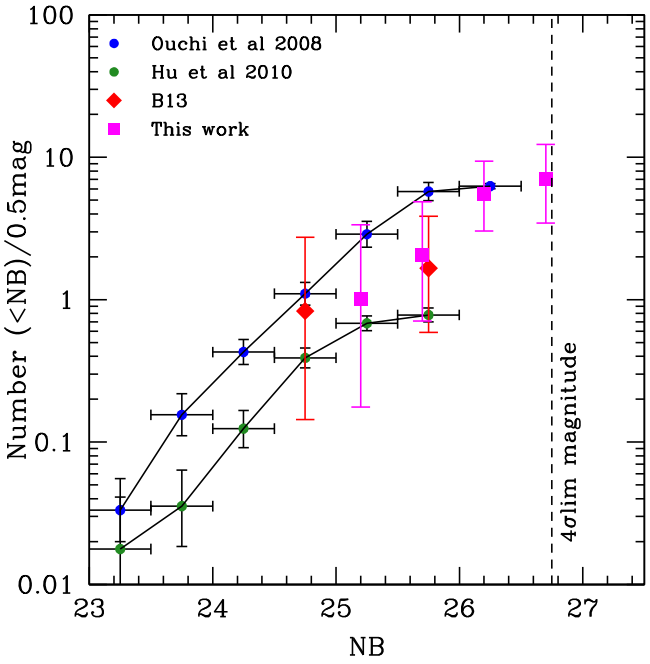

Figure 6. Cumulative number counts of LAEs observed in two blank fields, i.e., not containing quasars, by Ouchi et al. (2008) and Hu et al. (2010) (blue and green dots) and in the field of the $z = 5.7$ quasar ULAS J0203+0012 by B13 (red diamonds). All the number counts are rescaled to our effective area. We also show the 4σ limit magnitude in this work (dashed line). In the present study we retrieve six possible LAE candidates (magenta squares, see Section 3). The number counts of this work are corrected taking into account our completeness at the corresponding NB magnitudes. We have no evidence of an overdensity around the quasar. The errors reported are the poissonian noise for small counts (Gehrels 1986).

assess our ability to recover a population of galaxies that is gravitationally bound to the quasar.

We adopt a distribution of LAEs according to the luminosity function reported by Ouchi et al. (2008, with parameters $L^* = 6.8 \times 10^{42}$ erg s^{-1}, $\Phi^* = 7.7 \times 10^{-4}$ Mpc^{-3} and $\alpha = -1.5$). We then create a synthetic population of LAEs, drawing objects from the luminosity function through the Monte Carlo method. We modeled the LAEs as composed of a flat continuum emission ($L_{cont} = L_{Ly\alpha}/EW$) and a Ly$\alpha$ emission line, implemented as a Gaussian function, with a FWHM at restframe of 200 km s^{-1} (corresponding to typical line widths for LAEs, e.g., Ouchi et al. 2008). We account for the absorption due to the intergalactic medium using the reshift-dependent recipe given by Meiksin (2006), and assume an

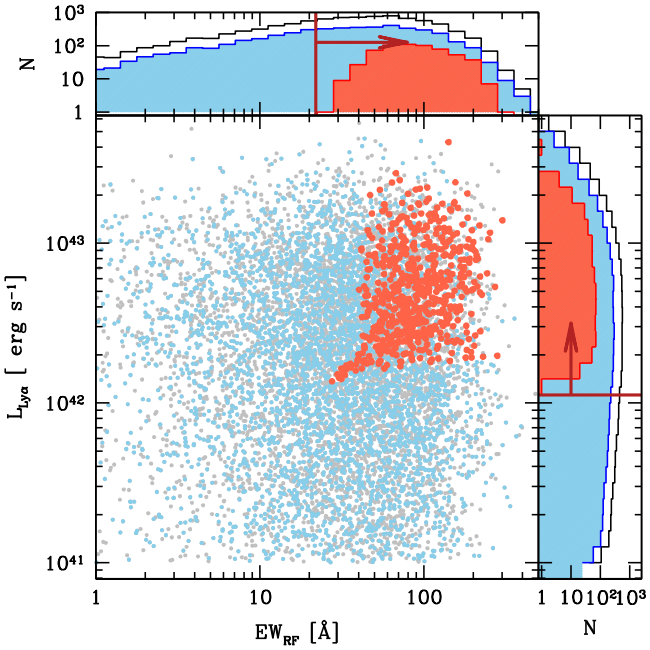

Figure 7. Equivalent width at restframe and Lyα luminosity of all our synthetic templates of LAEs (gray) of sources in the redshift range $5.61 < z < 5.77$ (blue) and of the sources detected as LAEs by our selection criteria (red points). The upper and right panels show the distribution of EW and Lyα luminosity, respectively. The red solid lines show the minimum retrieved EW and Lyα luminosity (25 Å and 1.32×10^{42} erg s^{-1}).

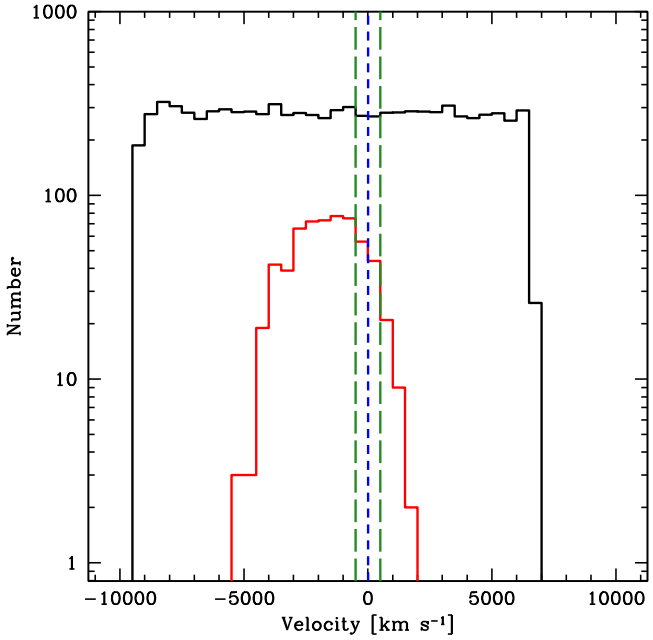

Figure 8. Velocity distribution of mock LAEs with respect to the systemic velocity of PSO J215–16 (short dashed blue line). In black we report the distribution of all the simulated sources, while in red we plot the sources recovered as LAEs. The velocity window encompassing $+500$ km s^{-1}/ -500 km s^{-1} with respect to the quasar is shown with long dashed green lines. The velocity window is not centered on the redshift of the quasar, but we still recover $\gtrsim$50% of the expected galaxy population that is gravitationally bound to the quasar.

exponential distribution of equivalent widths at restframe (Zheng et al. 2014, $N = e^{-\mathrm{EW}/50\,\text{Å}}$). Our mock spectra are randomly distributed in the redshift range $5.52 < z < 5.88$ and cover down to a luminosity of $L_{\mathrm{Ly}\alpha} = 10^{41}$ erg s^{-1}.

This results in synthetic magnitudes in the filters used in this work. We considered the sources detected with our NB image depth at the 4σ magnitude limit. We substituted the z and R broadband magnitudes with their respective 2σ limit magnitudes when their values were fainter than our detection limits. We considered the synthetic LAEs detected by our color selection criteria (see Section 3), and all the sources that were not detected in the two broad bands, but were detected in NB.

In Figure 7 we show the EW at restframe and Lyα luminosity distributions of all our generated LAEs of the subsample in the redshift range $5.6 < z < 5.78$ (the window in which we find LAEs in our simulation), and of LAEs recovered by the criteria presented in this study. We recover sources with a minimum EW at restframe of 25 Å and a Lyα luminosity of 1.32×10^{42} erg s^{-1}. The last value is in agreement with what is obtained when one calculates the limit $L_{\mathrm{Ly}\alpha}$ by considering that all the flux observed in the NB filter at our 4σ limit is due the line emission ($\sim 1.72 \times 10^{42}$ erg s^{-1}, see Appendix A).

We normalize the total number of simulated sources to the number of objects expected in a blank field in a cosmological volume equal to the one analyzed here, where we use a line-of-sight depth of 40 cMpc (see Section 1). By integrating the LAE luminosity function down to the Lyα luminosity limit considered in the simulation (10^{41} erg s^{-1}), we expect to measure 81.4 sources. Taking our depth and selection criteria into account, we recover 28% of the original sample. Therefore, we expect to observe $\sim$23 LAEs in a field with a cosmological volume that is the same as in our study. We selected six LAE candidates in our images; when we correct for a completeness level of 67% at our NB magnitude limit (see Figure 3), we obtain eight objects. This comparison suggests that the field surrounding PSO J215–16 might be less than $\sim$3 times less dense than the blank field, in agreement with what is shown in Figure 6.[6]

We report in Figure 8 the logarithmic distribution of the LAE systemic velocities with respect to the quasars, again for our entire simulated sample and for the objects detected as LAEs. The quasar is not located at the center of the redshift range covered by our selection. Nevertheless, we can still recover a significant fraction of galaxies even at the red edge. If we assume that LAEs that are gravitationally bound to the quasar are distributed following a Gaussian function centered on the quasar systemic velocity and a width of $\sigma \sim 500$ km s^{-1}, we calculate that given the shifted position of the quasar, we can recover 56% of the total LAE population. If we assume a velocity dispersion of $\sim$1000 km s^{-1}, our estimate decreases to 53%. Several studies (e.g., Hashimoto et al. 2013; Song et al. 2014) have suggested that the Lyα emission could be redshifted by $\sim$200 km s^{-1} with respect to the systemic velocity of the source. If this were the case, it would affect our results even more. Nevertheless, we find that the fraction of observed objects in this case would only decrease to 49% and 48% (in case of $\sigma = 500$ km s^{-1} and 1000 km s^{-1}, respectively). Thus, even in the most extreme scenario, we can still recover $\gtrsim$50% of the LAEs that are expected to be present in the proximity of PSO J215–16. However, it is necessary to consider that our observed counts are also affected by Poisson noise and cosmic variance. Trenti & Stiavelli (2008) provided estimates on the variance of the observed number counts,

[6] We note that Ouchi et al. (2008) states that their completeness level at their last luminosity bin (NB = 26) is estimated to be 50%–60%. Therefore, the last point of the blue curve in Figure 6 should be corrected accordingly.

taking into account both Poisson noise and cosmic variance, and they based their results on a variety of parameters (e.g., the survey volume and completeness, the halo filling factor, and expected number of objects)[7]. In our case, we consider a cosmological volume V given by our field of view and a redshift interval of $\Delta z \sim 0.16$, centered on $z = 5.69$ ($V \sim 14{,}900$ cMpc^3, see Figure 8); an intrinsic number of objects equal to the one recovered by our LAE simulation (23), a completeness of 67% (see Section 2 and Figure 3), and a Sheth-Tormen bias calculation. Kovač et al. (2007) studied the clustering properties of LAEs at $z \sim 4.5$ and found that the duty cycle of high-redshift LAEs varies within 6%–50%. We here consider both extreme cases. However, Kovač et al. (2007) considered a sample of LAEs with a minimum EW of 80 Å; since our EW limit is lower (25 Å, see Figure 7), we expect that the halo filling factor for our case is closer to 50%. Then, we expect to observe 15 ± 7 (9) sources in the case of a duty cycle of 6% (50%), where the fractional uncertainties due to cosmic variance and Poisson noise are 36% (49%) and 26% (in both cases), respectively. These results are consistent within 1.3σ in the first case and within 1σ in the second case with what is expected in the present study. Conversely, we can also obtain a rough estimate of the cosmic variance for a population of galaxies for which we know the expected number density in a certain volume, following Somerville et al. (2004). These authors used cold dark matter models to derive the expected bias (b) and root variance of the dark matter ($\sigma_{\rm DM}$) as a function of galaxy number density and survey volume, respectively (see their Figure 3). We consider our survey volume as reported above, and an expected number density obtained by integrating the LAE luminosity function until the Lyα luminosity limit from our simulation ($\sim 10^{-3}$ cMpc^{-3}); we derive a fractional cosmic variance of $\sigma_{\rm v} = b\sigma_{\rm DM} \sim 0.66$ for a population of galaxies at $z = 6$. This value is higher than what is recovered using the method illustrated by Trenti & Stiavelli (2008); however, the cosmic variance is not a trivial quantity to estimate and depends on several assumptions considered in the models, e.g., the LAE halo filling factor. Considering the latter value that we obtained, we would expect to detect 23 ± 15 sources, which, taking into account our completeness, is consistent within 1σ with the observations reported here. Moreover, considering a clustering scenario, e.g., consistent with the LAE–LAE clustering case (see Ouchi et al. 2003 and Section 6), we would obtain 26 ± 18 sources, which is consistent with the observed sources.

6. CLUSTERING

We may also study the environment of PSO J215–16 through a clustering approach. If quasars and galaxies are indeed clustered, then the excess probability of finding a galaxy at a distance r from a quasar with respect to a random distribution of sources can be estimated through the two-point correlation function (Davis & Peebles 1983):

$$\xi(r) = (r/r_0)^{-\gamma}, \tag{4}$$

where r_0 and γ are the correlation length and clustering strength, respectively. In order to account for redshift distortions on the line of sight, we can instead consider the volume-averaged projected correlation function. This is ξ(r) integrated over a line-of-sight distance $d = 2v_{\rm max}/aH(z)$ (with $v_{\rm max}$ the maximum velocity from the quasar) and within a radial bin of width $[R_{\rm min}, R_{\rm max}]$ (Hennawi et al. 2006):

$$\overline{W}(R_{\rm min}, R_{\rm max}) = \frac{\int_{-d/2}^{d/2}\int_{R_{\rm min}}^{R_{\rm max}} \xi(\mathrm{r})\, 2\pi dR dr}{V}, \tag{5}$$

where V is the volume of the cylindrical shell:

$$V = \pi(R_{\rm max}^2 - R_{\rm min}^2)d. \tag{6}$$

Therefore, the number of galaxies that we expect to find around a quasar within a volume V in the presence of clustering is

$$\mathrm{NC} = N(1 + \overline{W}(R_{\rm min}, R_{\rm max})). \tag{7}$$

In case of no clustering, the number of sources expected is

$$N = nV, \tag{8}$$

where n is the number density of galaxies per cMpc^{-3} above a certain limit in luminosity. In this scenario, N is equal to the number of galaxies found in a blank field within a cosmological volume V.

In this study, we calculate n by integrating the LAE luminosity function (Ouchi et al. 2008) down to the luminosity limit obtained by our simulation (1.32×10^{42} erg s^{-1}, see Section 5). We consider a line-of-sight distance given by $v_{\rm max} = 4000$ km s^{-1} (consistent with the interval probed by our NB selection, see Sections 1 and 5, and Figure 8), $R_{\rm min} = 0.001$ cMpc and increasing values of $R = R_{\rm max}$.

In Figure 9 we show the number of galaxies expected as function of R in case of no clustering (Equation (8)) and in different scenarios of quasar-galaxy clustering (Equation (7)). Since there are currently no studies of LAE-quasar clustering at high redshift, we consider for comparison some other illustrative cases. We take values of r_0 and γ that have been obtained by observations of galaxy-quasar clustering at lower-z and LAE–LAE and quasar–quasar clustering at $z \sim 5$. Indeed, studies of galaxy-quasar clustering at $z \sim 1$ (Zhang et al. 2013) have estimated $r_0 = 6$ h^{-1} cMpc and $\gamma = 2.1$.[8] Ouchi et al. (2003) derived the clustering properties of LAE at $z = 4.86$ from a sample of objects detected in the Subaru Deep Field, for which they obtained $r0 = 3.35$ h^{-1} cMpc and $\gamma = 1.8$. At high redshift, constraints on the quasar–quasar clustering properties are given by the discovery of a close bright quasar pair, with only 21″ separation, at $z \sim 5$ (McGreer et al. 2016). The correlation function derived from this pair gives $r_0 > 20$ h^{-1} cMpc and $\gamma = 2.0$.[9] We show the number of LAEs found in this study. We also report the objects recovered by B13 and the number of sources expected in their study in case of no clustering (since their observations are shallower than those presented here, with a Lyα luminosity limit of 3.74×10^{42} erg s^{-1}, the number of expected background sources is lower). Our number counts are consistent with a scenario of no clustering (i.e., the background counts, in line with what is obtained in

[7] http://casa.colorado.edu/~trenti/CosmicVariance.html

[8] We note, however, that the galaxies studied by Zhang et al. (2013) are not selected as LAEs but by considering all the sources in the quasar field recovered in the SDSS-Stripe 82 catalog that are brighter (in the i band) than a certain threshold value, which depends on the field depth. This selection also includes passive and red galaxies.

[9] These values are in agreement with those found by Shen et al. (2007, $r0 = 25.0$ h^{-1} cMpc and $\gamma = 2$) based on a sample of lower redshift ($z > 3.5$) bright SDSS quasars. However, we note that other quasar clustering studies, such as Eftekharzadeh et al. (2015), have suggested much smaller clustering scales, with $r0 = 7.59$ h^{-1} cMpc (obtained from a lower luminosity quasar sample, $z \sim 3.4$; see also Section 7).

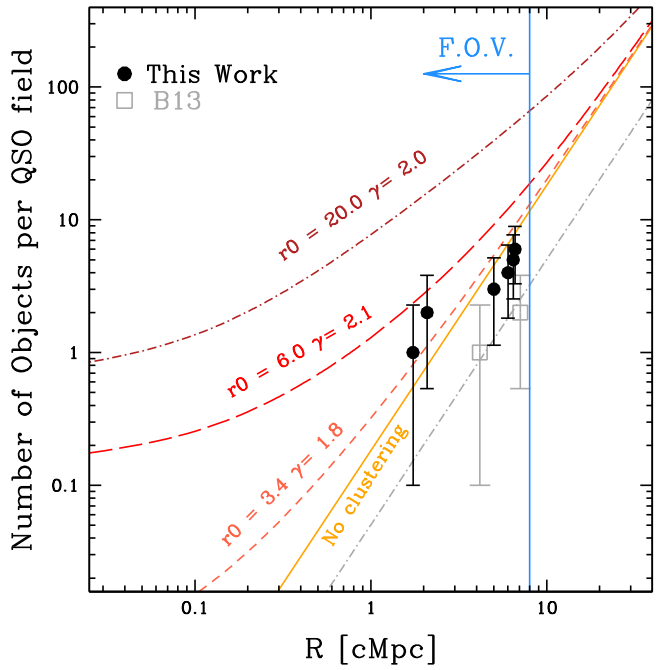

Figure 9. Expected number of LAEs, given the depth reached in this study, as a function of projected distance from the quasar, in case of no clustering (e.g., a random distribution of sources, yellow solid line), and for some illustrative clustering scenarios, taken from observational studies (Zhang et al. 2013; Ouchi et al. 2003 and McGreer et al. 2016, short dash, long dash and dot-short-dash line, respectively, see text for details). The counts of LAEs observed in this study are reported (not corrected for completeness). We also report the LAEs found by B13 and their expected number of sources in case of no clustering, taking into account the depth of their study (dot-long-dash line). For the sake of clarity, we do not report the respective cases of clustering scenarios. We show the field of view (FOV) encompassed by our study. The errors are the Poissonian noise on small counts from Gehrels (1986). The counts of the observed LAEs are consistent with what is expected in a blank field.

Section 4), and do not show evidence of strong clustering in either of the two quasar fields.

7. DISCUSSION

We do not find evidence of an overdensity of LAEs in an area of $\sim$37 arcmin^2 centered on the $z = 5.73$ quasar PSO J215–16. Here we investigate possible scenarios to explain our findings.

1. *The overdensity is more extended than our field of view.* Overzier et al. (2009) and more recently Muldrew et al. (2014) used a combination of *N*-body simulations and semi-analytical models. They have found that overdensities of galaxies at $z \sim 6$ are expected to be very extended and can cover regions up to $\sim$25–30 arcmin radius, corresponding to $\gtrsim$20 pMpc at that redshift. In the present study we only cover a region with a transversal radius of $\sim$1 pMpc, and we might be missing a large part of a potential overdensity. We would like to stress that under the hypothesis that the quasar occupies the center of a $z \sim 6$ overdensity similar to the one found by Toshikawa et al. (2014) in a blank field, searches in area of $\sim$2–3 pMpc should still show evidence of an enhancement in the number of galaxies with respect to a blank field.

   From an observational perspective, enhancements in the number of galaxies around quasars have been reported on rather modest scales, comparable to ours or even smaller. However, there are indications, based on LBGs searches, that some quasars are surrounded by overdensities on larger scales, even if additional spectroscopic confirmation is needed (see Section 1).

   In Table 2 we show a summary of the findings obtained by diverse studies, which considered different areas and techniques.

   In our case, in order to discard or confirm this scenario, we would need further observations covering a wider area (e.g., with a radius of $\gtrsim$20 arcmin).
2. *The ionizing emission from the quasar prevents structure formation in its immediate proximities.* Strong radiation from a bright quasar can ionize its nearby regions (up to $\sim$1–5 pMpc radius around $z \sim 6$ quasars, e.g., Venemans et al. 2015), with an increase in both the temperature and ionized fraction of the intergalactic medium (IGM), and in the intensity of the local UV radiation field.

   The effects on the visibility of the Lyα radiation in this region are not straightforward to deduce. As a consequence of the increase in the UV background radiation field, a higher Lyα transmission flux value is expected around the quasar with respect to the typical IGM environment at the same redshift (Bruns et al. 2012). However, in addition to the rise in the UV background, the nearby IGM temperature also increases. Thus, the isothermal virial temperature necessary for gas accretion in the dark matter halo is higher, and the mass needed to form a structure increases (Jeans-mass filtering effect, Gnedin 2000). Even if the Lyα transmission flux is assumed to be higher, the formation of galaxies itself is suppressed, especially for objects at the low-mass end (e.g., Shapiro et al. 2004). Utsumi et al. (2010) invoked this effect in order to explain the absence of galaxies in a region with a radius of $\sim$3 pMpc around a $z \sim 6$ quasar (see Section 1 and Table 2). Given the typical sizes of ionized regions in quasars, and because we here only cover scales of $\sim$2 pMpc, suppression of galaxy formation that is due to the quasar ionizing radiation might explain the lack of LAEs.
3. *The bulk of the overdensity population is composed of dusty/obscured galaxies.* Observations find that host galaxies of $z > 5$ quasars contain a considerable amount of dust ($\sim 10^8$–$10^9\,M_\odot$) and molecular gas ($\sim 10^{10}\,M_\odot$, see Carilli & Walter 2013 for a review). They are already characterized by a metal-enriched medium, comparable to what is observed at low redshift (e.g., De Rosa et al. 2011). One might foresee that the galaxies assembling in the proximity of the quasar might also be characterized by a high dust/molecular gas content. Indeed, Yajima et al. (2015) implemented a 3D radiation transfer code in a high-resolution cosmological simulation to show that overdense regions at $z \sim 6$, where quasars are expected to be found, host more evolved, disk-like, and massive ($M_{\rm star} \sim 10^{11}\ M_\odot$) galaxies than an average field at the same redshift. These galaxies are characterized by a strong dust extinction (i.e., a low UV radiation escape fraction, $f_{\rm esc} \lesssim 0.1$), and a powerful star formation (SFR $\gtrsim 100\,M_\odot\,{\rm yr}^{-1}$); therefore they are very bright in the IR, with $L_{\rm IR}$ as high as $\sim 4 \times 10^{12}\,L_\odot$. These massive and highly obscured objects, whose detection in the UV restframe might be hindered by absorption and/or be

Table 2
List of $z > 5$ Quasars Whose Large-scale Fields Were Inspected for the Presence of Galaxy Overdensities

Object	Redshift	References	Instrument	FoV (cMpc^2)	FoV (pMpc^2)	Overdensity
ULAS J0203+0012	5.72	(7)	VLT FORS2	250	5.6	0
SDSS J0338+0021	5.03	(6)	VLT FORS2	250	5.6	+
SDSS J0836+0054	5.82	(3)	*HST* ACS	65	1.4	+
SDSS J1030+0524	6.28	(1)	*HST* ACS	65	1.4	+
		(2)	GMOS-N	170	3.7	0
		(4)	*HST* ACS	65	1.4	+
		(9)	LBT LBC	3136	64.0	+
SDSS J1048+4637	6.20	(2)	GMOS-N	170	3.7	0
		(4)	*HST* ACS	65	1.4	0
		(9)	LBT LBC	3136	64.0	+
ULAS J1120+0641	7.08	(8)	*HST* ACS	65	1.4	0
SDSS J1148+0356	6.41	(2)	GMOS-N	170	3.7	0
		(4)	*HST* ACS	65	1.4	−
		(9)	LBT LBC	3136	64.0	+
SDSS J1204–0021	5.03	(6)	VLT FORS2	250	5.6	+
SDSS J1306+0356	5.99	(4)	*HST* ACS	65	1.4	−
SDSS J1411+1217	5.95	(9)	LBT LBC	3136	64.0	+
SDSS J1630+4012	6.05	(4)	*HST* ACS	65	1.4	+
CFHQS J2329–0301	6.43	(5)	Subaru SuprimeCam	4600	83.3	+
CFHQS J0050+3445	6.25	(10)	*HST* ACS & WFC3	29	0.6	−
PSO J215.1512–16.0417	5.73	(11)	VLT FORS2	206	4.5	0

Note. We report the quasar names, redshifts, literature references, instruments used, and area covered in each study (in comoving and physical Mpc^2 at $z \sim 6$). The references are coded as (1) Stiavelli et al. (2005), (2) Willott et al. (2005), (3) Zheng et al. (2006), (4) Kim et al. (2009), (5) Utsumi et al. (2010), (6) Husband et al. (2013), (7) Bañados et al. (2013), (8) Simpson et al. (2014), (9) Morselli et al. (2014), (10) McGreer et al. (2014), and (11) this work. All these studies, except for Bañados et al. (2013) and this work, which searched for LAEs, are based on i-dropout selection. We also report whether the fields were found to be overdense (+), underdense (−), or consistent (0) with respect to a comparison blank field. We note cases in which the same field was found consistent with a blank field when inspected on small scales, while overdense when studied over larger scales (e.g., SDSS J1048+4637 and SDSS J1148+0356). The overdensity reported by Utsumi et al. (2010), even if found with the Subaru SuprimeCam, spreads across an area of ∼3 Mpc radius, therefore it would also have been detected by searches over smaller fields of view.

strongly dependent on orientation effects, rather than LAEs (i.e., young dust-poor star-forming galaxies), may be a more suitable tracer for high-redshift massive overdensities.

Further studies of the environment of high-redshift quasars with submillimeter facilities (in particular ALMA, which has successfully detected $z \sim 6$ field galaxies, e.g., Capak et al. 2015; Willott et al. 2015) would permit us to test this scenario, allowing us to recover a possible population of dusty galaxies in the quasar field. However, we note that owing to the small field of view of ALMA (with a size of $\sim 20''$, corresponding to ∼800 ckpc ∼110 pkpc at $z \sim 6$), we would only be able to search the most proximate region around the quasar. A recent study of the fields around three $z > 6.6$ quasars with ALMA did not find an excess of dusty galaxies in a region of 65 ckpc radius (Venemans et al. 2016).

4. *Quasars at high redshift do not inhabit massive dark matter halos.* The quasar two-point correlation function at low redshift ($z \lesssim 2.5$), as derived from both the 2dF QSO Redshift Survey (Croom et al. 2005) and the SDSS (Ross et al. 2009) quasar sample, shows that quasars are commonly associated with average-mass dark matter halos (i.e., $M_{\rm DMH} \sim (2\text{–}3) \times 10^{12}\,M_{\odot}$), far less massive than the most massive halos at the same redshift ($\sim 10^{14}$–$10^{15}\ M_{\odot}$), independently of the quasar luminosity.

At higher z ($3.5 \lesssim z \lesssim 5.4$), the scenario is less clear: based on the SDSS sample, Shen et al. (2007) have calculated an average dark matter host halo mass of $(4\text{–}6) \times 10^{12}\,M_{\odot}$, slightly higher than the results at lower redshifts. However, more recent studies, based on the final SDSS III-BOSS quasar sample, did not find a clear evolution of quasar clustering from $z \sim 0$ to $z \sim 3$ (Eftekharzadeh et al. 2015).[10]

From a theoretical point of view, there have been studies suggesting that quasars at high redshift ($z \gtrsim 5$) also inhabit dark matter halos with average masses (i.e., less massive than the most massive halos at that epoch). In particular, Fanidakis et al. (2013) performed simulations based on the semi-analytical model GALFORM, in order to study the relation between quasars and dark matter halos up to $z \sim 6$. They showed that in case of models in which AGN feedback is considered, the masses of the dark matter host halos are roughly $\sim 10^{12}\,M_{\odot}$, from $z \sim 0$ to $z \sim 6$: this is an order of magnitude lower than the most massive halos at $z \sim 6$ obtained in the same simulation, and is in agreement with observations at low redshift. However, as argued by Simpson et al. (2014), it is worth noting that the simulations by Fanidakis et al. (2012) failed to create the most massive black holes ($M \gtrsim 10^9\,M_{\odot}$) at $z \sim 6$, while

[10] We note that the quasars considered here are less massive than those studied by Shen et al. (2007).

they appear only at $z \sim 4$. Therefore, the claims reported here are to be taken with caution, and may not hold in every scenario.

8. CONCLUSIONS

We studied the environment of the $z = 5.73$ quasar PSO J215–16 searching for LAEs using broadband and narrowband VLT imaging, on Mpc-scales, i.e., ∼2 pMpc ∼14 cMpc at the redshift of the quasar. This is the second study in which we do not find evidence of an overdensity of Lyα emitting sources in a quasar field, compared to blank fields (see also B13). These results may be explained by a variety of different scenarios (i.e., the overdensity is spatially more extended than our field of view, or galaxy formation is prevented by the ionizing radiation of the quasar, or the galaxies in the field are mainly dusty, or the quasar is not central to a massive dark matter halo in the early universe).

Studies on wider areas (>20 arcmin radius, corresponding to ∼8 pMpc ∼ 47 cMpc at the redshift of the quasar), with the support of additional multiwavelength observations (i.e., IR/submillimeter), are required in order to distinguish among these scenarios.

However, it is intriguing to note that overdensities of galaxies around radio-loud sources (both radio-loud galaxies and AGN) have been extensively reported (e.g., Venemans et al. 2007; Wylezalek et al. 2013) throughout a wide redshift range ($0 < z < 4$), and for several cases even at $z \gtrsim 5.2$ (Venemans et al. 2004; Zheng et al. 2006). In the future, it appears to be worthwhile to repeat our experiment on $z > 6$ radio-loud quasars, whose sample has recently been substantially increased (Bañados et al. 2015), to potentially target the earliest galactic structures.

Based on observations made with the ESO Telescope at the La Silla Paranal Observatory, under program ID 091.A-0677(A).

B.P.V., E.P.F., and F.W. acknowledge funding through the ERC grant "Cosmic Dawn." Support for R.D. was provided by the DFG priority program 1573 "The physics of the interstellar medium." Support for R.O. was provided by CNPq programs 459040/2014-6 and 400738/2014-7. C.M. thanks the IMPRS for Astronomy & Cosmic Physics at the University of Heidelberg. C.M. thanks N. Fanidakis, L. Morselli, C. Garcia, R. Gilli, and M. Onoue for useful discussion on this project.

Facility: VLT:Antu(FORS2).

APPENDIX A
STAR FORMATION RATE ESTIMATES OF LAE CANDIDATES

We infer here an SFR estimate for our possible LAE candidates. We use as SFR tracer the luminosity of the Lyα emission line.

We obtain the integrated luminosity of the Lyα line from the flux density observed in the narrowband filter ($f_{\rm NB}$):

$$L_{\rm Ly\alpha} = f_{\rm NB}\, 4\pi d_L^2\, \Delta\nu_{\rm NB}, \quad (9)$$

where d_L is the luminosity distance at the redshift of the quasar and $\Delta\nu_{\rm NB}$ is the width of the narrowband filter.

In this estimate, we do not correct for the contribution of the continuum, which is expected to be very faint (none of our LAE candidates are detected in the broad bands).

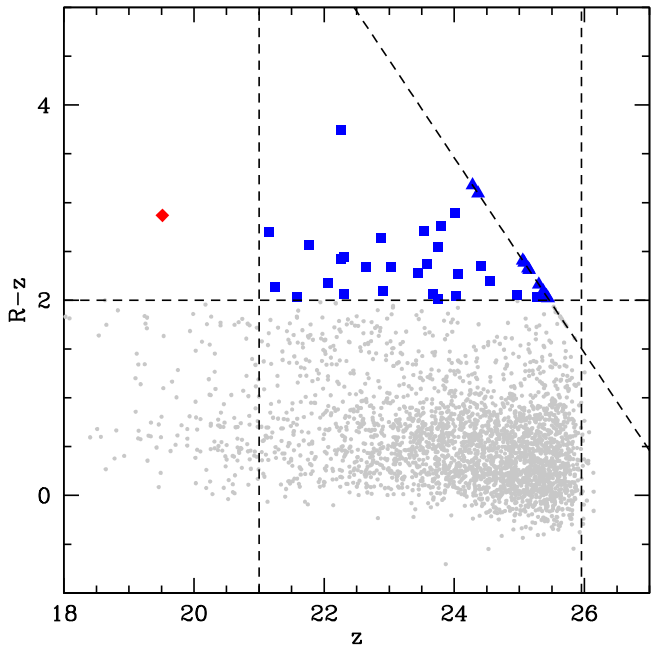

Figure 10. Color–magnitude diagram (R–z) vs. z. Gray points show all the sources detected in our field, considering the z frame as reference. The LBG candidates found from the z frame (37) are reported as blue squares. We show the lower limit on the z magnitude ($z > 21$) and the 5σ upper limit ($z = 25.96$) with vertical dashed lines. The horizontal line highlights our color criteria. The diagonal dashed line displays the 2σ limit magnitude in the R frame. The objects not detected in the R frame at 2σ level are reported as blue triangles. The red diamond shows the quasar position.

From $L_{\rm Ly\alpha}$ we can derive the luminosity of the Hα emission line ($L_{\rm H\alpha}$). Assuming case-B recombination (Osterbrock 1989), the conversion is given by $L_{\rm Ly\alpha} = 8.7 \times L_{\rm LH\alpha}$. Then, we use the following relation between SFR and $L_{\rm H\alpha}$ (Kennicut & Evans 2012):

$$\log \frac{\rm SFR_{Ly\alpha}}{M_\odot\ {\rm yr}^{-1}} = \log \frac{L_{\rm H\alpha}}{\rm erg\ s^{-1}} - 41.27. \quad (10)$$

We obtain SFR estimates in the range between (1.2 ± 0.2)–$(3.2 \pm 0.3)\, M_\odot\, {\rm yr}^{-1}$ (all the SFR values, together with the respective $L_{\rm Ly\alpha}$, are reported in Table 1) In all our analysis, we do not consider possible absorption that is due to the galactic dust. Even if LAEs are thought to be rather dust-poor objects (e.g., Garel et al. 2015), there has been evidence of a non-negligible fraction of dusty LAEs (Pentericci et al. 2009). The geometry and dynamic of the interstellar neutral gas also significantly contributes to the effective Lyα photon escape fraction. Indeed, a higher $L_{\rm H\alpha}/L_{\rm Ly\alpha}$ ratio is expected in case of a lower Lyα photon escape fraction. Finally, we neglect the effect of the significantly neutral intergalactic medium at the high redshift under consideration.

All these effects contribute to reducing the estimated SFRs: the values reported here can therefore only be considered as lower limits.

APPENDIX B
LYMAN-BREAK GALAXY ANALYSIS

In addition to the LAE selection, we also search for LBGs using the dropout technique. Since LBGs are expected to be

Table 3
Field Names, Coordinates, Effective Areas, and Technical Characteristics for the R and z Filters of our Comparison Fields and the Field Studied here

Field	R.A. (J2000.0)	Decl. (J2000.0)	Effective Area (arcmin^2)	$\lambda_{c,R}$ (Å)	$\Delta\lambda_R$ (Å)	$\lambda_{c,z}$ (Å)	$\Delta\lambda_z$ (Å)	Instrument	Reference
AEGIS	14:18:36.00	+52:39:0.00	88	6245	1232	8872	1719	MegaCam@CFHT	(1), (2)
COSMOS	10:00:31.00	+02:24:0.00	154	6245	1232	8872	1719	MegaCam@CFHT	(1), (2)
GOODS-N	12:35:54.98	+62:11:51.3	93	6276	1379	9028	1411	SuprimeCam@Subaru	(3)
UDS	02:17:49.00	−05:12:2.00	192	6508	1194	9060	1402	SuprimeCam@Subaru	(4)
B13	02:03:32.38	00:12:29.06	44	6550	1650	9100	1305	FORS2@VLT	(5)
This work	14:20:36.39	−16:02:29.94	37	6550	1650	9100	1305	FORS2@VLT	(6)

Note. The areas analyzed in this study and in B13 differ as a result of the diverse masking. References from the literature are (1) Hildebrandt et al. (2009), (2) Erben et al. (2009), (3) Capak et al. (2004), (4) Furusawa et al. (2008), (5) Bañados et al. (2013), and (6) this work.

characterized by a strong UV continuum, which is observed in the z filter, we use the catalog obtained taking the z frame as our reference image. We consider all the sources with S/N > 4 in z, and we apply only a selection using the broadband filters: we require a red R–z color (R–$z > 2$) and, since we expect galaxies at these redshift to be faint, we require $z > 21$.

We recover 37 LBG candidates: we report the color–magnitude (R–z) versus z in Figure 10. It is worth noting that in the selection of LBG candidates, we are mainly limited by the depth of the R image ($R_{2\sigma} = 27.46$) rather than by the depth of the z image; indeed, the faintest sources with $(R_{2\sigma} - z) > 2$ would have $z \leqslant 25.46$ in our analysis ($z_{5\sigma,\mathrm{lim}} = 25.96$).

For comparison, we refer to the works by Brammer et al. (2012) and Skelton et al. (2014), who compiled catalogs for some well-known extragalactic fields, completed with spectroscopic and photometric information. We consider four fields that can be used as comparison blank fields for our study: the All-wavelength Extended Groth Strip International Survey (AEGIS), the Cosmic Evolution Survey (COSMOS), the Great Observatories Origins Survey Northen field (GOODS-N), and the UKIRT InfraRed Deep Sky Survey (UKIDSS) Ultra Deep Field (UDS).

We selected LBG candidates from the catalogs by imposing the same selection criteria as in the present study. In order to account for the different image depths, we considered only sources with z and R magnitude lower than the limits in our field ($z < z_{5\sigma,\mathrm{lim}} = 25.96$ and $R < R_{2\sigma,\mathrm{lim}} = 27.46$). The GOODS-N and UDS fields are shallower than our images in both R and z and only in the z frame, respectively. In these cases, we took as limits the corresponding values provided by Skelton et al. (2014) ($z_{5\sigma,\mathrm{lim,GOODSN}} = 25.5$, $R_{2\sigma,\mathrm{lim,GOODSN}} = 27.19$ and $z_{5\sigma,\mathrm{lim,UDS}} = 25.9$).

We also considered the sample of LBG candidates recovered by B13 around ULAS J0203+0012 (20 sources), where they used a selection method analogous to the method described here. They reached limit magnitudes in the z and R bands of $z_{5\sigma,\mathrm{lim,B13}} = 25.14$ and $R_{2\sigma,\mathrm{lim,B13}} = 27.29$.

In Table 3 we report information on the comparison fields and on our field, i.e., coordinates, effective areas, literature references, and characteristics of R and z filters. Although the different fields were imaged with slightly different filter sets, the redshift windows covered are large ($\Delta z \sim 1.2$) and corresponding to the window spanned in the present study.[11]

[11] With the filters used, we span $5.2 \lesssim z \lesssim 6.3$ and $\Delta z \sim 1.1$ in the AEGIS and COSMOS fields, $5.2 \lesssim z \lesssim 6.4$ and $\Delta z \sim 1.2$ in the GOODS-N field, and in the UDS field, we reach $5.4 \lesssim z \lesssim 6.5$ and $\Delta z \sim 1.1$. In the present study and in B13 we selected sources in $5.2 \lesssim z \lesssim 6.5$ and $\Delta z \sim 1.3$.

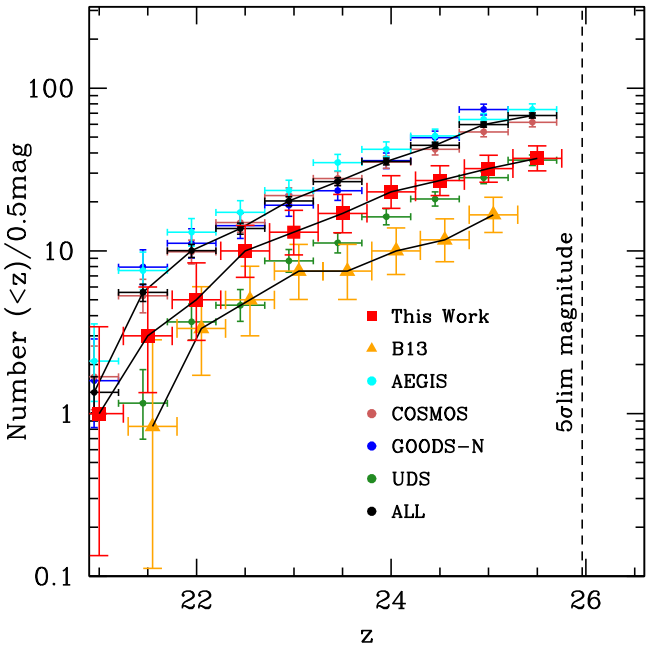

Figure 11. Cumulative number counts of LBGs at $z \sim 6$. All the counts are scaled for the effective area in our study. We report the candidates found around the $z = 5.73$ quasar PSO J215–16 (red squares) and the quasar ULAS J0203+0012 (orange triangles, B13), slightly shifted with respect to the other fields in order to avoid confusion. We show the sources that were selected using the same selection criteria and image depth in four comparison blank fields (AEGIS as cyan, COSMOS as brown, GOODS-N as blue, and UDS as green circles). The result obtained considering all the blank fields together is shown with black circles. The errors are taken from the Poisson noise in case of low counts statistics (Gehrels 1986).

We report the cumulative number counts, scaled to our effective area, of the sources found in the four blank fields and around the quasars (Figure 11). The difference between the counts obtained in the UDS field with respect to the counts in the other blank fields may be due to a diverse contribution of contaminant sources. Indeed, the UDS field was imaged through an R filter that was slightly redder than the filters used in the other fields (see Table 3): this might turn into a more conservative selection of high-redshift LBGs. Recent studies have also suggested that the UDS field might be intrinsically underdense in $z \sim 6$ galaxies with respect to other well-known fields (Bowler et al. 2015; Bouwens et al. 2015).

We can compare the cumulative number counts of LBGs in the field of the quasar studied here with the counts found in the comparison blank fields. In order to avoid incompleteness

Table 4
Field Names, Total Number of LBG Candidates Retrieved by Our Photometric Cuts, and Number of Sources with Photometric Redshift Estimates Corresponding to $z_{\rm phot} \geqslant 5$

Field	Number LBGs	Number Phot LBGs
AEGIS	176	11
COSMOS	257	26
GOODS-N	186	7
UDS	187	17

issues at the low-luminosity end, we take only sources with $R < R_{\rm lim,5\sigma}$, considering the GOODS-N field, which is the shallowest of our fields ($R_{\rm lim,5\sigma} = 26.2$). Taking into account our color selection criterion, we obtain a resulting z magnitude limit of 24.2. At this limit, the counts of the LBG candidates in our quasar field is consistent within 1σ with the counts in the UDS field, and lower than the counts in the AEGIS, COSMOS, and GOODS-N fields by $\sim$1.7, 1.3, and 1.1σ, respectively. The quasar field analyzed here appears only marginally ($\sim 1.1\sigma$) denser than the field studied in B13. These results are hence in agreement with B13, where no overdensity of LBGs with respect to a blank field was found.

Some general caveats are to be taken into account. Considering our broad selection criteria, both our sample and the samples derived from the comparison fields might be contaminated by red sources with lower redshift. We employ the further information provided in the catalogs of the comparison fields in order to better characterize the sources retrieved by our LBGs selection. We can consider the available photometric redshift estimates, computed with the public code EAZY (Brammer et al. 2008), which take into account all the photometric information present in the catalog. We take only the objects with a reliable redshift estimate, as based on the quality parameter Q_z ($Q_z < 2.0$, see Brammer et al. 2008), and for which $z_{\rm phot} \geqslant 5.0$. Only the 6%, 10%, 4%, and 9% of the LBG sample from the AEGIS, COSMOS, GOODS-N, and UDS field, respectively, could be identified as high-redshift galaxies (see Table 4), while the vast majority were better fitted by a $z \sim 1$ galaxy model. This simple test shows how the selection criteria used here, without the help of further bands, lead us to a highly contaminated sample.

In summary, the LBG selection also does not reveal a possible overdensity around the quasar. However, because of the wide redshift range we considered, an enhancement in the number of LBGs in the quasar field would represent an indication, more than solid evidence, of the presence of an overdensity of galaxies in the proximity of the quasar.

REFERENCES

Angulo, R. E., Springel, V., White, S. D. M., et al. 2012, MNRAS, 425, 2722
Appenzeller, I., & Rupprecht, G. 1992, Msngr, 67, 18
Bañados, E., Venemans, B., et al. 2015, ApJ, 804, 118
Bañados, E., Venemans, B., Decarli, R., et al. 2016, arXiv:160803279B
Bañados, E., Venemans, B., Morganson, E., et al. 2014, AJ, 148, 14
Bañados, E., Venemans, B., Walter, et al. 2013, ApJ, 773, 178
Barth, A. J., Martini, P., Nelson, C. H., & Ho, L. C. 2003, ApJ, 594L, 95
Begelman, M. C., Volonteri, M., & Rees, M. J. 2006, MNRAS, 370, 289
Bertin, E., & Arnouts, S. 1996, A&AS, 117, 390
Bond, J. R., Arnett, W. D., & Carr, B. J. 1984, ApJ, 280, 825
Bouwens, R. J., Illingworth, G. D., Oesch, P. A., et al. 2015, APJ, 803, 34
Bowler, R. A. A., Dunlop, J. S., McLure, R. J., et al. 2015, MNRAS, 452, 1817
Brammer, G. B., van Dokkum, P. G., & Coppi, P. 2008, ApJ, 686, 1503
Brammer, G. B., van Dokkum, P. G., Franx, M., et al. 2012, ApJS, 200, 13
Bruns, L. R., Wyithe, J. S. B., Bland-Hawthorn, J., & Dijkstra, M. 2012, MNRAS, 421, 2543
Capak, P. L., Carilli, C., Jones, G., et al. 2015, Natur, 522, 455
Capak, P. L., Cowie, L. L., Hu, E. M., et al. 2004, AJ, 127, 180
Carilli, C. L., & Walter, F. 2013, ARA&A, 51, 105
Carnall, A. C., Shanks, T., Chehade, B., et al. 2015, MNRAS, 451L, 16
Chiang, Y. K., Overzier, R., Gebhardt, K., et al. 2013, ApJ, 779, 127
Croom, S. M., Boyle, B. J., Shanks, T., et al. 2005, MNRAS, 356, 415
Davis, M., & Peebles, P. J. E. 1983, ApJ, 267, 465
De Rosa, G., Decarli, R., Walter, F., et al. 2011, ApJ, 739, 56
Decarli, R., Walter, F., Yang, Y., et al. 2012, ApJ, 756, 150
Devecchi, B., & Volonteri, M. 2009, ApJ, 694, 302
Eftekharzadeh, S., Myers, A., White, M., et al. 2015, MNRAS, 453, 2798
Erben, T., Hildebrandt, H., Lerchster, M., et al. 2009, A&A, 493, 1197
Fan, X., Strauss, M. A., Becker, R. H., et al. 2006, AJ, 132, 117
Fanidakis, N., Baugh, A. V., Benson, A. J., et al. 2012, MNRAS, 419, 279
Fanidakis, N., Macciò, A., Baugh, A. V., et al. 2013, MNRAS, 436, 315
Ferrarese, L. 2002, ApJ, 578, 90
Finkelstein, K., Finkelstein, S., & Vithal, T. 2015, ApJ, 813, 78
Finkelstein, S., Rhoads, J., Malhotra, S., & Grogin, N. 2009, ApJ, 691, 465
Furusawa, H., Kosugi, G., Akiyama, M., et al. 2008, in ASP Conf. Ser. 399, Panoramic Views of Galaxy Formation and Evolution, ed. T. Kodama et al. (San Francisco, CA: ASP), 131
Garel, T., Blaizot, J., Guiderdoni, B., et al. 2015, MNRAS, 450, 1279
Gehrels, N. 1986, ApJ, 303, 336
Gnedin, N. Y. 2000, ApJ, 542, 535
Hashimoto, T., Ouchi, M., Shimasaku, K., et al. 2013, ApJ, 765, 70
Heahnelt, M. G., & Rees, M. J. 1993, MNRAS, 263, 168
Hennawi, J., Strauss, M. A., Oguri, M., et al. 2006, AJ, 131, 1
Hildebrandt, H., Pierloz, J., Erben, T., et al. 2009, A&A, 498, 725
Hu, E., Cowie, L. L., Barger, A. J., et al. 2010, ApJ, 725, 394
Husband, K., Bremer, M. N., Stanway, E. R., et al. 2013, MNRAS, 432, 2869
Jahnke, K., & Macció, A. 2011, ApJ, 734, 92
Kennicut, R. C., & Evans, N. J. 2012, ARA&A, 50, 531
Kim, S., Stiavelli, M., Trenti, M., et al. 2009, ApJ, 695, 809
Kovač, K., Somerville, R., Rhoads, J. E., et al. 2007, ApJ, 668, 15
Lang, D., Hogg, D.-W., Mierle, K., Blanton, M., & Roweis, S. 2010, AJ, 139, 1782
Latif, M. A., & Schleicher, D. R. G. 2015, A&A, 578A, 118
Magnier, E. A., Schafly, E., Finkbeiner, D., et al. 2013, ApJS, 205, 20
Maiolino, R., Cox, P., Caselli, P., et al. 2005, A&A, 440L, 51
McGreer, I., Eftekharzadeh, S., Myers, A. D., & Fan, X. 2016, AJ, 151, 61
McGreer, I., Fan, X., Strauss, M., et al. 2014, AJ, 148, 73
Meiksin, A. 2006, MNRAS, 365, 807
Morganson, E., De Rosa, G., Decarli, R., et al. 2012, AJ, 143, 142
Morselli, L., Mignoli, L., Gilli, R., et al. 2014, A&A, 568A, 1
Mortlock, D. J., Warren, S. J., & Venemans, B. 2011, Natur, 474, 616
Muldrew, S. I., Hatch, N. A., & Cooke, E. A. 2014, MNRAS, 452, 2528
Ono, Y., Ouchi, M., Shimasaku, K., et al. 2010, ApJ, 724, 1524
Osterbrock, D. E. 1989, Astrophysics of Gaseous Nebulae and Active Galactic Nuclei (Mill Velly, CA: Univ. Science Books)
Ouchi, M., Shimasaku, K., Akiyama, M., et al. 2008, ApJS, 176, 301
Ouchi, M., Shimasaku, K., Furusawa, H., et al. 2003, ApJ, 582, 60
Overzier, R. A., Guo, Q., Kauffmann, G., et al. 2009, MNRAS, 394, 577
Pentericci, L., Grazian, A., Fontana, A., et al. 2009, A&A, 494, 553
Pirzkal, N., Malhotra, S., Rhoads, J. E., & Xu, C. 2007, ApJ, 667, 49
Riechers, D. A., Walter, F., Bertoldi, F., et al. 2009, ApJ, 703, 1338
Ross, N. P., Shen, Y., Strauss, M. A., et al. 2009, ApJ, 697, 1634
Sarkar, P., Yadav, J., Pandey, B., & Bharadwa, S. 2009, MNRAS, 399L, 128
Schlafly, E. F., & Finkbeiner, D. P. 2011, ApJ, 737, 103
Shapiro, P. R., Iliev, I. T., & Raga, A. C. 2004, MNRAS, 348, 753
Shen, Y., Strauss, M. A., Oguri, M., et al. 2007, AJ, 133, 2222
Simpson, C., Mortlock, D., Warren, S., et al. 2014, MNRAS, 442, 3454
Skelton, R. E., Whitaker, K. E., Momcheva, I. G., et al. 2014, ApJS, 214, 24
Somerville, R., Kyoungsoo, L., Ferguson, H. C., et al. 2004, ApJ, 600L, 171
Song, M., Finkelstein, S. L., Gebhardt, K., et al. 2014, ApJ, 791, 3
Springel, V., White, S. D. M., Jenkins, A., et al. 2005, Natur, 435, 629
Steidel, C. C., Giavalisco, M., Pettini, M., Dickinson, M., & Adelberger, K. L. 1996, ApJ, 462L, 17
Stiavelli, M., Djorgovski, S. G., Pavlovsky, C., et al. 2005, ApJ, 622L, 1
Toshikawa, J., Kashikawa, N., Overzier, R., et al. 2014, ApJ, 792, 15
Trenti, M., & Stiavelli, M. 2008, ApJ, 676, 767
Utsumi, Y., Goto, T., Kashikawa, N., et al. 2010, ApJ, 721, 1680

Venemans, B., Bañados, E., Decarli, R., et al. 2015, ApJ, 801L, 11
Venemans, B., Findlay, J. R., Sutherland, W. J., et al. 2013, ApJ, 779, 24
Venemans, B., Röttgering, H. J. A., Miley, G. K., et al. 2007, A&A, 461 823
Venemans, B., Röttgering, H. J. A., Overzier, R. a., et al. 2004, A&A, 424L, 17
Venemans, B., Walter, F., Zschaechner, L., et al. 2016, ApJ, 816, 37
Volonteri, M. 2010, A&ARv, 18, 279
Walter, F., Bertoldi, F., Carilli, C., et al. 2003, Natur, 424, 406
Willott, C. J., Carilli, C., Wagg, J., & Wang, R. 2015, ApJ, 807, 180
Willott, C. J., Delorme, P., Omont, A., et al. 2010, AJ, 139, 906
Willott, C. J., Percival, W. J., McLure, R. J., et al. 2005, ApJ, 626, 657
Wu, K. K. S., Lahav, O., & Rees, M. J. 1999, Natur, 397, 225
Wyithe, J. S. B., & Loeb, A. 2003, ApJ, 595, 614
Wylezalek, D., Galametz, A., Stern, D., et al. 2013, ApJ, 769, 79
Yajima, H., Shlosman, I., Romano-Diaz, E., & Nagamine, K. 2015, MNRAS, 451, 418
Zhang, S., Wang, T., Wang, H., & Zhou, H. 2013, ApJ, 773, 175
Zheng, W., Overzier, R. A., Bouwens, R. J., et al. 2006, ApJ, 640, 574
Zheng, Z. Y., Wang, J. X., Malhotra, S., et al. 2014, MNRAS, 439, 1101